Computational Fluid Dynamics Modeling of Nitric Oxide Transport in a Rat Mesenteric Lymphatic Vessel

John T. Wilson[1], Wei Wang[2], Augustus H. Hellerstedt[1], David C. Zawieja[2], James E. Moore Jr.[1]

[1]Department of Biomedical Engineering
Texas A&M University
5045 Emerging Technologies Building
3120 TAMU
College Station, TX 77843, USA
Tel: 979-845-5532
Fax: 979-845-4450

[2]Department of Systems Biology and Translational Medicine
Texas A&M Health Science Center
702 Southwest H.K. Dodgen Loop
Temple, TX 76504, USA
Tel: 254-742-7033
Fax: 254-742-7145

INTRODUCTION

The lymphatic system is an expansive vascular network that plays a vital role in fluid homeostasis and physiologic function within the body. It is responsible for the transport of fluid from the interstitial spaces to the venous return. Its dysfunction could result in a number of pathologies including lymphedema, or swelling within the interstitial spaces. Additionally, it is important for proper immune system functionality and macromolecular balances.

Terminal lymphatics composed primarily of endothelial cells passively take up fluid, cells, debris, and solutes from the interstitial spaces. Eventually, this initial network of vessels gives rise to the collecting lymphatics which are generally tubular vessels segmented by bi-leaflet check valves encapsulated by a bulbous sinus region. Lymph (largely aqueous with relatively low concentrations of proteins and cells compared to blood) is propelled through the collecting lymphatics via two primary modes: intrinsic and extrinsic mechanisms. The former, also known as active pumping, is the result of lymphatic muscle cell contraction, while the latter involves external compression mechanisms such as the movement of skeletal muscle or other tissues surrounding the lymphatic.

Nitric oxide (NO), a known vasodilator, has been shown to influence lymphatic pumping. Enhanced wall shear stress (WSS) has been shown to activate eNOS in lymphatic endothelial cells (LECs), cells that cover the vessel wall, to produce NO during *in situ* lymphatic vessel experiments [1]. Bohlen *et al.* found an approximately 2-4 fold higher concentration of NO in the bulbous surface of the valve region of the lymphatics compared to that of the tubular portion [1, 2]. The mechanisms behind this difference in concentration are not clear. The answer to this question may lie in the nature of flow patterns in lymphatic vessels and/or the shear sensitivity of LECs.

While there are no studies that have attempted to model transport within the lymphatic system, several computational works have been conducted that model NO transport within a parallel plate flow chamber or a simplified model of the microcirculation [3-5]. Despite the 2-D nature of these models, they provided valuable insight with regard to theoretical framework (e.g. constant parameter and non-dimensionalization) that aided in the development of the model presented herein. Other models developed for the lymphatic system are simply lumped-parameter [6, 7], one-dimensional [6, 7], or do not properly take into account the geometry of the valve region [8].

The main aim of this study was to characterize the distribution of NO within a physiologic model of a lymphatic vessel obtained from confocal images in response to various convective flow regimes and degrees of LEC sensitivity to shear. In particular, we wanted to identify the importance of the convective transport of NO within the lymphatic vasculature and determine if the high concentrations in the sinus region observed in an experimental setting may be attributed to flow-mediated factors, higher LEC numbers, or some combination. While there have been experimental studies that have quantified NO concentration within the lymphatics [1], to our knowledge this is the first study that has attempted to computationally model the transport of NO within a 3-D model of a lymphatic vessel.

METHODS

Stacks of confocal images of a rat mesenteric lymphatic vessel (obtained during previous imaging experiments) were imported into Scan IP/FE (Simpleware, Exeter, UK) and were smoothed, filtered, and reconstructed into a 3-D surface mesh of the vessel fluid region (Fig. 1). In particular, recursive Gaussian and salt-and-pepper filters were used to smooth the images and

reduce noise. The surface mesh was then saved in *.stl format for later computational fluid dynamics (CFD) analysis.

Employing the analogy between mass and energy transfer, the dimensionless temperature values were used to model the concentration of NO in the vessel. To ensure accuracy in our analysis, the Lewis relation [9] was employed and α/D_{ij} was specified as unity, where α is thermal diffusivity and D_{ij} is the diffusion coefficient of NO in aqueous solution. Thus, the energy solutions had the same shape as that of the mass transfer. All mass transfer values were matched from the literature [4] and correspond to NO in aqueous solution. Hence, all computational details described hereafter will only involve concentration values.

Steady simulations were performed using the commercially available software Star-CCM+ (v7.04.006,CD-adapco, Melville, NY). The thermal results were non-dimensionalized to obtain the analogous concentration solution. Lymph was assumed to be a Newtonian and incompressible fluid with a dynamic viscosity, μ, of 0.9 cP and density, ρ, of 1 g cm^{-3}. Transport of NO is governed by the Advection-Diffusion-Reaction equation:

$$\frac{\partial C_{NO}}{\partial t} = -\vec{v} \bullet \vec{\nabla} C_{NO} + D_{ij} \vec{\nabla}^2 C_{NO} - k_{NO} C_{NO}^2 , \quad (1)$$

where $\vec{v}$ is the velocity field, C_{NO} is the concentration of NO, t is time, and k_{NO} is the pseudo-second order auto-oxidative NO reaction rate. A sigmoidal relationship between NO production and axial WSS was used as the flux boundary condition for NO production at the wall of the vessel (Eq. 2):

$$R_{NO}(r) = \frac{R_{NO,Max}}{1 + \gamma \exp(-W_o \left| WSS_{axial} \right|)} \quad (2)$$

where R_{NO} is the production rate of NO, $R_{NO,Max}$ is the maximum production rate of NO corresponding to the rate used by Plata *et al*. [4] when modeling arterial endothelial cell production, WSS_{axial} is axial WSS, r is the radius, and γ and W_o characterize LEC sensitivity to shear. This function represents an increase in NO production in response to WSS, but at a certain value of axial WSS (termed the "saturation point") the LECs can no longer produce at a higher rate with further elevation in shear (Fig. 2). Furthermore, an increase or decrease in the parameter W_o results in this saturation point occurring at a higher or lower value of axial WSS. In this study, W_o was varied to determine the effect of different saturation points on the concentration of NO within the lumen of the vessel. Simulations were also run using constant NO production boundary conditions with dimensionless values of 0.09 and 0.5 corresponding to the parameters B1 and B5, respectively.

Variables were converted to dimensionless for using analysis similar to that of Plata *et al*. resulting in the following dimensionless equation:

$$\frac{\partial C^*}{\partial t^*} = -Pe\vec{v}^* \bullet \vec{\nabla} C^* + \vec{\nabla}^2 C^* - k_{NO}^* C^{*2}, \qquad (3)$$

where Pe is the Peclet number equilavant to $2RV_o/D_{ij}$ and V_o is the average inlet velocity.

Model Geometry and Computational Inputs

200 μm long inlet and outlet extensions were added to the geometry to facilitate the application of boundary conditions. The extrusion lengths were varied to determine the effect on velocity and concentration within the lumen of the vessel and it was found that the lengths aforementioned were optimal. In particular, the selected inlet length allowed for the development of a 3-D parabolic velocity profile. The velocity profile was implemented at the inlet with

average velocities ranging from 0.5-7.0 mm s^{-1} that are in the physiologic range of velocities observed during *in situ* experiments [10] (Table 1). Note the Reynolds number, Re, is defined as $\rho V_o 2R/\mu$.

A static concentration of C^*_{NO} =0.3 corresponding to a dimensional concentration of 100 nM was applied as a Dirichlet boundary condition at the inlet of the vessel. The outlet concentration was extrapolated from adjacent core cells using a reconstruction gradient. The extruded walls of the entrance and exit regions of the vessel were set to a zero flux in order to prevent interaction with concentration profiles within the physiologically relevant portion of the geometry. Residuals were allowed to reach a value on the order of 10^{-4} to ensure convergence.

Mesh Independence

Mesh independence was investigated by comparing steady flow axial WSS values (fully developed inlet condition) in meshes with 95,149, 201,056, 385,080, and 1,202,744 volumetric cells (Fig. 3). Less than 6% RMS error in axial WSS was found between the 385,080 and 1,202,744 cell meshes, which compares well with the criteria set forth by Ethier *et al.* in modeling flow in coronary arteries [11]. Therefore, the 385,080 cell mesh was used for all results.

RESULTS

Velocity streamlines revealed areas of flow stagnation adjacent to the valve leaflets in the sinus region (Fig. 4). While flow features in this region appear to be vortex-like in shape, it should be noted that the absolute value of velocities in this region were less than 0.03 mm s^{-1} compared to an average inlet velocity of 2.0 mm s^{-1}.

The maximum shear stress occurred near the inner surface of the trailing ends of the lymphatic valve leaflets and was 12.0 dyne cm^{-2} for an imposed Pe value of 91 (Fig. 5). Contours of NO production (Fig. 6 Left and Right) revealed higher production in areas of elevated WSS dictated by the sigmoidal function used for the flux boundary condition of NO. When W_o was set to a lower value (Fig. 6 Left), the LECs were less sensitive to shear compared to simulations run at a higher value of W_o (Fig. 6 Right). Higher values of W_o (W_o=1.14) resulted in an LEC saturation of production occuring at approximately 7.7 dyne cm^{-2} (Fig. 6 Right), while lower values of W_o (W_o=0.2) resulted in much lower sensitivity with a saturation value occuring at 39.5 dyne cm^{-2} (Fig. 6 Left).

Despite higher production levels in the simulations run with large Pe values, the prodominant role of convective forces was evident from the diminished concentration within the lumen of the vessel. The highest concentrations were found near the backside of the valve leaflet insertions in areas of flow stagnation and low WSS (Fig. 7 Top, Middle, and Bottom). Simulations run at lower Pe numbers (Fig. 7 Top) resulted in higher concentrations than those run at elevated Pe values (Fig. 7 Bottom).This may be attributable to NO being washed out of the lumen of the vessel due to higher convective forces.

The flow-mediated decrease in concentration was also evident in the areas of flow stagnation near the valve leaflets. After $Pe \geq 61$, the concentration at the wall did not change substantially as is evident by comparing the two simulations run at the higher Pe values ($\leq 3.7\%$ difference) (Fig. 7 Middle and Bottom Panels).

DISCUSSION

The study presented herein investigated the effects of fluid dynamics and LEC shear-sensitivity on the concentration of NO within the lumen of a lymphatic vessel. To our knowledge, there are no previous studies of this nature conducted on a model obtained from confocal images of a live lymphatic vessel. By implementing shear-sensitive boundary conditions for the production of NO, we were able to understand how the sensitivity of LECs may play a role in the concentration of NO throughout the vessel. Additionally, we showed that areas of high concentration exist within the sinus regions near the valve leaflets as observed by Bohlen *et al*. [1].

While the average values of shear within the lymphatic flow regime are approximtely 0.64 dyne cm^{-2} in the tubular region [10], the peak values of shear quantified in simulations at the inner surface of the valve leaflets were generally comparable to WSS values calculated for large arteries [12]. Additionally, high concentrations have been observed experimentally near the valve leaflets in the sinus area, but it was unclear whether this phenomenon was due to high surface area with more LECs to produce NO, higher production rates in general at this site, or whether it is flow mediated. Furtheremore, experiments have shown that an increase in shear results in increased production of NO by LECs in whole lymphatic vessels [1]. We found that LECs in areas of flow stagnation observed in representative velocity streamlines produced NO at a much lower rate than do LECs in the higher shear areas of the vessel. Despite the low production rates in this area, there was substantially more NO present in this region compared to areas of high production, suggesting the high concentration in this area observed experimentally is flow-mediated and due to fluid stagnation as opposed to a higher amount of NO production by LEC in this part of the vessel. Additionally, the extremely low levels of production and highly

diffusive effects may outweigh the concept that high surface area of LECs is the sole cause of the enhanced NO levels.

A few limitations should be noted when considering this model. The geometry used for all simulations was static while in reality lymphatic vessels contract and expand dramatically over time, thus the results included in this research are limited to steady conditions in a stationary domain. The viscous nature of the fluid and laminar flow characteristics suggest this movement may be negligible and a quasi-static approach is appropriate, however future work could include dynamic movement of the valve leaflets to validate this assumption. Future work could also include incorporation of diffusion through the vessel wall. Consequently, it would be useful to determine whether the areas of high concentration such as as those found adjacent to the valve leaflets due to flow stagnation would have the highest amount of diffusion through the vessel wall. This type of analysis would be dependent on the diffusivity of NO within the vessel wall.

Our results showed that high concentrations observed adjacent to the valve leaflets in experimental findings were most likely due to flow-mediated processes. Because higher values of shear led to increasing concentrations at the wall only after Pe was at or above approximately 61, simulations suggested that this value was where convective forces start to greatly affect the concentration distribution.

In short, the concentrations of NO within the lymphatic vesssel were found to be sensitive to changes in the convective scheme and LEC sensitivity. Further studies could be conducted to investigate the fully dynamic system of NO transport resulting from vessel wall movement and valvular propulsion of lymph.

REFERENCES

[1] Bohlen, H. G., Wang, W., Gashev, A., Gasheva, O., and Zawieja, D., 2009, "Phasic Contractions of Rat Mesenteric Lymphatics Increase Basal and Phasic Nitric Oxide Generation in Vivo," American Journal of Physiology-Heart and Circulatory Physiology, 297(4), pp. H1319-H1328.

[2] Bohlen, H. G., 2011, "Nitric Oxide Formation by Lymphatic Bulb and Valves Is a Major Regulatory Component of Lymphatic Pumping," American journal of physiology. Heart and circulatory physiology, 301(5), pp. H1897.

[3] Fadel, A., Barbee, K., and Jaron, D., 2009, "A Computational Model of Nitric Oxide Production and Transport in a Parallel Plate Flow Chamber," Annals of biomedical engineering, 37(5), pp. 943-954.

[4] Plata, A., Sherwin, S., and Krams, R., 2010, "Endothelial Nitric Oxide Production and Transport in Flow Chambers: The Importance of Convection," Annals of biomedical engineering, 38(9), pp. 2805-2816.

[5] Vaughn, M. W., Kuo, L., and Liao, J. C., 1998, "Effective Diffusion Distance of Nitric Oxide in the Microcirculation," American Journal of Physiology-Heart and Circulatory Physiology, 274(5), pp. H1705-H1714.

[6] Bertram, C., Macaskill, C., and Moore Jr, J., 2011, "Simulation of a Chain of Collapsible Contracting Lymphangions with Progressive Valve Closure," Journal of biomechanical engineering, 133(1), pp. 011008.

[7] Reddy, N. P., Krouskop, T. A., and Newell, P. H., 1977, "A Computer Model of the Lymphatic System," Computers in biology and medicine, 7(3), pp. 181-197.

[8] Rahbar, E., and Moore, J. E., 2011, "A Model of a Radially Expanding and Contracting Lymphangion," Journal of biomechanics, 44(6), pp. 1001-1007.

[9] Incropera F.P., D. D. P., Bergman T.L., Lavine L.S., 2007, *Fundamentals of Heat and Mass Transfer*, John Wiley, Hoboken, NJ.

[10] Dixon, J. B., Greiner, S. T., Gashev, A. A., Cote, G. L., Moore, J. E., and Zawieja, D. C., 2010, "Lymph Flow, Shear Stress, and Lymphocyte Velocity in Rat Mesenteric Prenodal Lymphatics," Microcirculation, 13(7), pp. 597-610.

[11] Myers, J., Moore, J., Ojha, M., Johnston, K., and Ethier, C., 2001, "Factors Influencing Blood Flow Patterns in the Human Right Coronary Artery," Annals of biomedical engineering, 29(2), pp. 109-120.

[12] Moore, J. E., Xu, C., Glagov, S., Zarins, C. K., and Ku, D. N., 1994, "Fluid Wall Shear Stress Measurements in a Model of the Human Abdominal Aorta: Oscillatory Behavior and Relationship to Atherosclerosis," Atherosclerosis, 110(2), pp. 225-240.

TABLES

Table 1. Range of velocities and dimensionless numbers used for steady simulations. Note that Re is less than one for all cases, suggesting the important role of viscous forces in the lymphatic flow regime.

Re	Pe	Vo ($mm\ s^{-1}$)
0.06	15	0.5
0.11	30	1.0
0.22	61	2.0
0.33	91	3.0
0.44	121	4.0
0.56	152	5.0
0.67	182	6.0
0.78	212	7.0

FIGURES

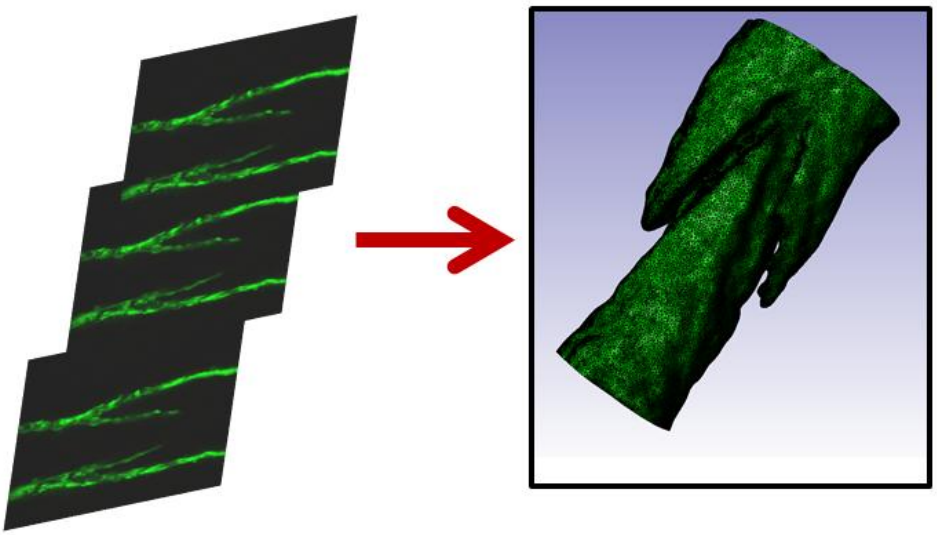

Figure 1. Confocal images of the wall of the rat mesenteric lymphatic vessel (left) along with reconstructed geometry of the fluid region (right). 200 μm extensions (extensions not shown in illustration) were added at both the inlet and outlet of the vessel to accommodate flow simulations.

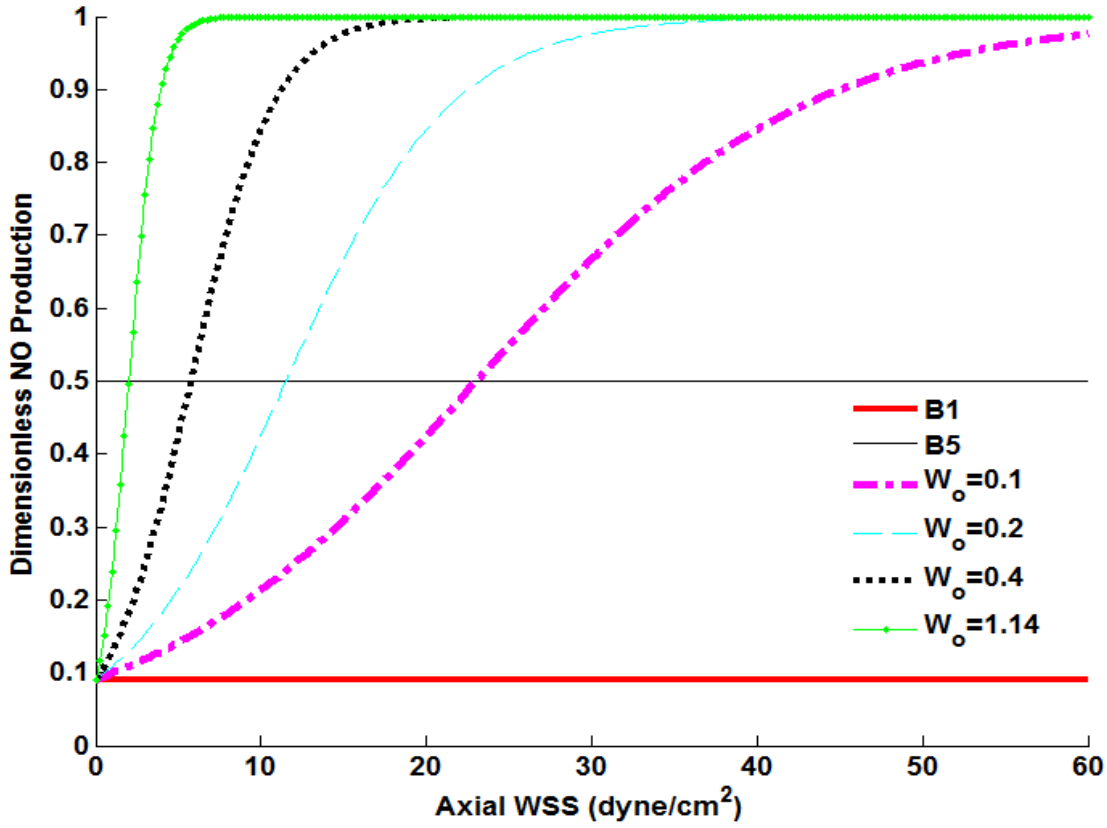

Figure 2. Range of NO production values fixed with γ=10. For shear dependent cases, W_o was varied from 0.1 to 1.14 corresponding to increasing levels of LEC shear-sensitivity. Basal level productions B1 and B5 correspond to dimensionless production values of 0.09 and 0.5, respectively.

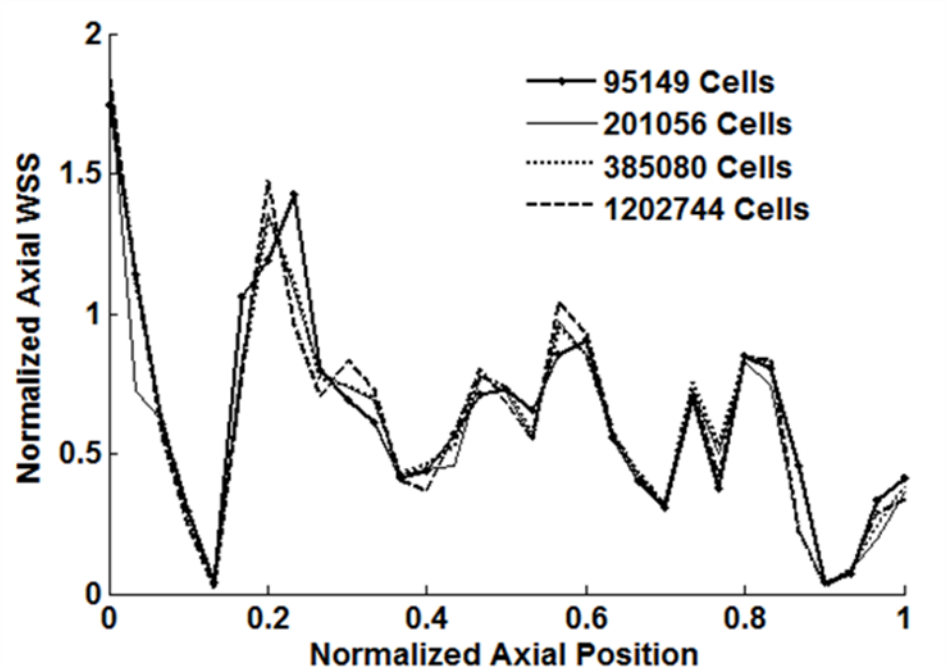

Figure 3. Mesh indpendence study using WSS as convergence criteria in the rat mesenteric lymphatic vessel. The steady WSS values were normalized by the inlet Poiseuille flow value of WSS and plotted along the wall of the vessel. A parabolic inlet velocity was used in each case.

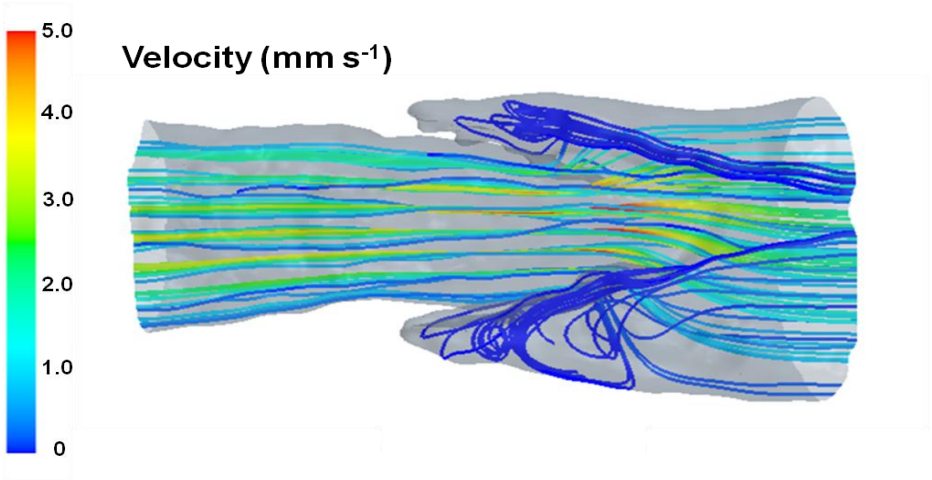

Figure 4. Representative streamlines for a simulation run at Re=0.22. Areas of flow stagnation were observed adjacent to the valve leaflets. Although these appear vortex-like in nature, these are regions of essentially zero velocity.

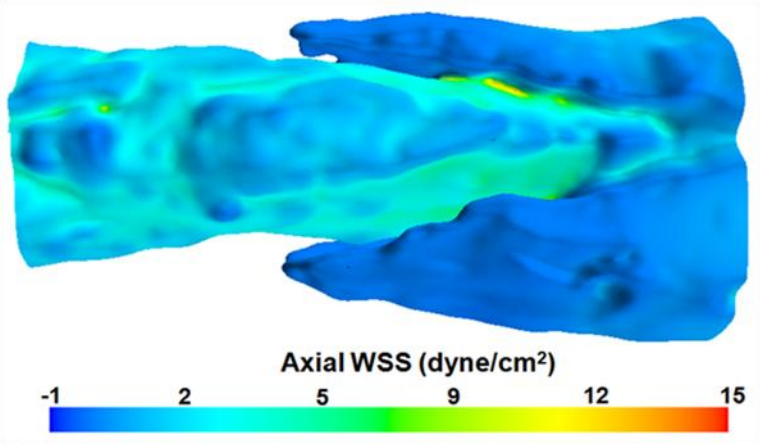

Figure 5. Distribution of axial WSS for Pe=91.

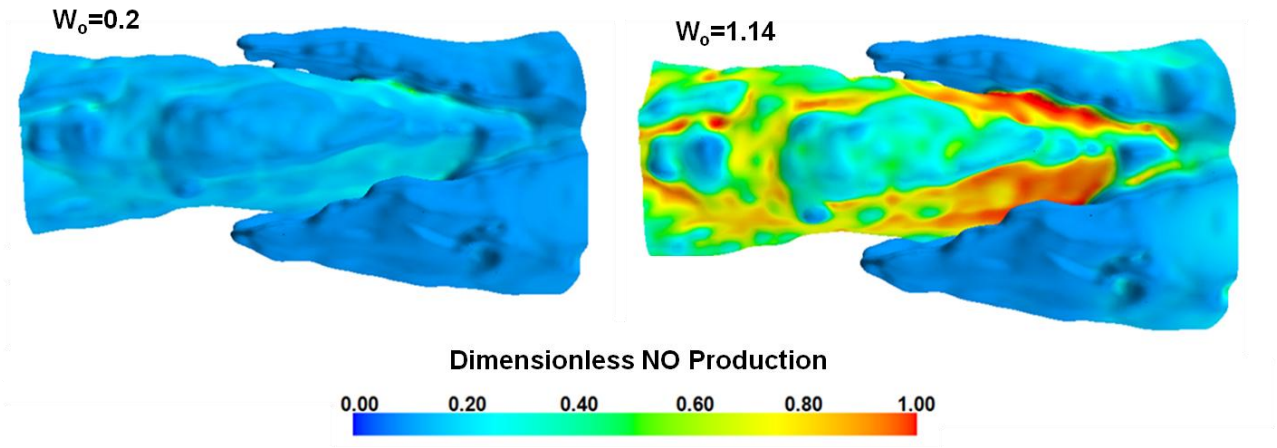

Figure 6. Left: Dimensionless NO Production for Pe=91 and W_o=0.2; Right: Dimensionless NO Production for Pe=91 and W_o=1.14.

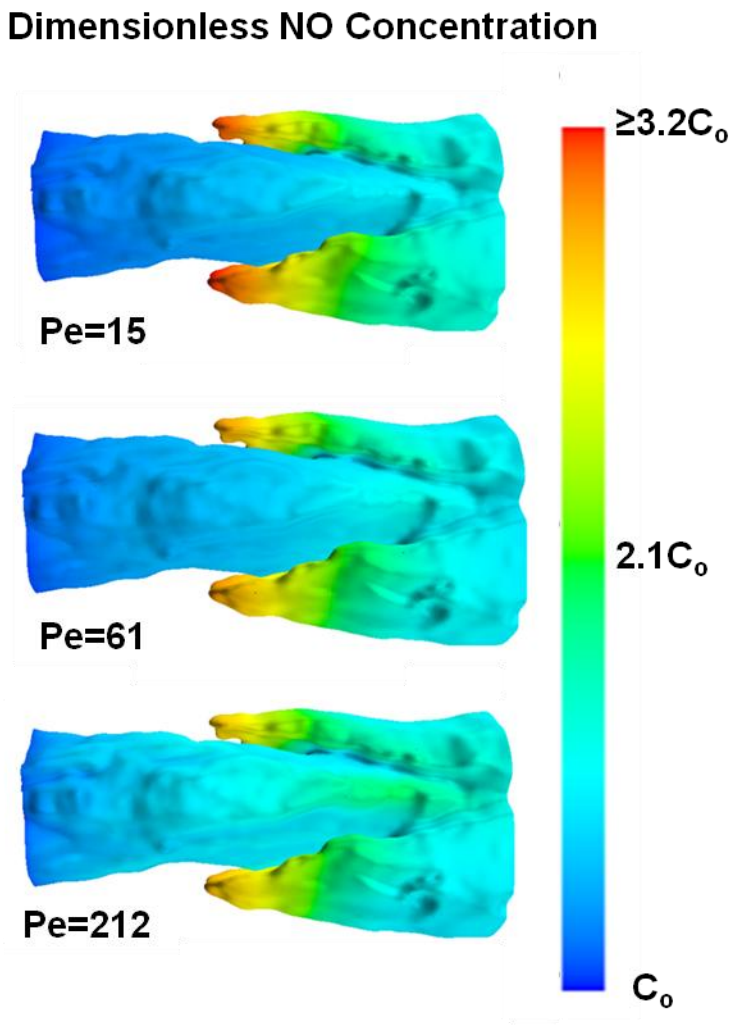

Figure 7. Contours of NO at the wall of the vessel for various Pe values. Top: Surface concentration for Pe=15 and W_o=1.14; Middle: Surface concentration for Pe=61 and W_o=1.14; Bottom: Surface concentration for Pe=212 and W_o=1.14. Increasing the average Pe value resulted in less wall concentration, however enhanced Pe values beyond Pe=61 up until Pe =212 only resulted in an RMS percent difference in NO concentration of 3.7%.